Thermal evolution and exhumation of the Ladakh Batholith, northwest Himalaya, India

Thermal evolution and exhumation of the Ladakh Batholith, northwest Himalaya, India

Linda A. Kirstein;

School of GeoSciences, University of Edinburgh, West Mains Road, Edinburgh EH9 3JW, U.K.

Key words: Ladakh; geobarometry; amphibole; thermochronology; tectonics.

Abstract

High elevation, low relief regions are recognised across the northwest Himalaya, including the Ladakh and Kohistan areas. A homogeneity of uplift and cooling histories across these large spatial (>360 km) and temporal (>35 million years) scales would be remarkable. Here we examine the thermal evolution of the Ladakh Batholith, northwest India since the early Tertiary using a combination of amphibole geobarometry and apatite and zircon low temperature thermochronometry data to investigate the spatio-temporal progression of emplacement, uplift and exhumation. The emplacement depth varies with distance north of the Indus River and suggests that the southern part of the batholith (< 10 km from the Indus River) had more overlying rocks removed (~3-5 km more) compared to the northern edge. Compiled low temperature thermochronometry data from elevations >3200 m above mean sea level indicate significant exhumation of the southern margin of the Ladakh Batholith in the Oligocene (> 26 Ma) while exhumation of the northern margin occurred later in the Mid to Late Miocene (<17 Ma). Topography across the batholith was asymmetric throughout the Oligocene and Miocene and potentially only since the Pliocene has the current amplitude and wavelength been established. This extensive dataset from across the Ladakh Batholith does not support a generalised regional model of early rapid exhumation post India-Eurasia collision followed by steady and slow denudation to the present.

1. Introduction

Understanding the rise of plateau such as the Tibetan or Colorado plateaux has generated much research using a broad spectrum of techniques yet their origins remain elusive. In a recent study it was proposed that high-elevation, low-relief areas in the northwest Himalaya, from Kohistan in the west to the Karakoram fault in the east, are dismembered parts of the Tibetan Plateau which underwent a single, spatially uniform phase of surface uplift and denudation in the Eocene (50-40 Myr) with slow steady cooling since that time (van der Beek et al., 2009). Across such a large geographic area the potential for significant temporal and spatial heterogeneity in uplift and denudation is great, yet limited selected low temperature thermochronometer studies suggest otherwise (de Sigoyer et al., 2000; Kumar et al., 2007; van der Beek et al., 2009). Here we combine high temperature Al-in-hornblende pressure data with extensive, published low temperature thermochronometry (fission track and (U-Th)/He) data (Kirstein et al., 2009) to develop a model of the thermal evolution of part of the Transhimalayan Batholith, the Ladakh Batholith since emplacement in Cretaceous – Palaeogene times.

The Transhimalayan Batholith lies in the south and west parts of the Tibetan Plateau and is the remains of an Andean- type arc that extends for ~2500 km from Afghanistan in the west to Bhutan in the east (Fig. 1). This Cretaceous-Palaeogene (110-40 Ma) magmatic arc system formed by subduction of the Neotethys Ocean along the southern margin of Eurasia (Schärer et al., 1984), and today lies 100-200 km north of the High Himalaya. The Transhimalayan Batholith is exposed at elevations > 3200 m above mean sea level. Emplacement of the batholith in Ladakh may have resulted from two distinct phases of plutonism in the Cretaceous (ca. 103-80 Ma) and early Palaeogene (ca. 65-46 Ma) (Wen et al., 2008). Collision of India and Eurasia occurred in the Eocene and subduction related magmatism ceased from ~ 47 Ma (St-Onge et al., 2010).

The Ladakh Batholith, India, lies between the western margin of the modern Tibetan Plateau and the western Himalayan syntaxis. Morphological analyses indicate that the Ladakh region is characterised by widespread summit regions with low slopes (Jamieson et al., 2004; van der Beek et al., 2009). The batholith has been studied in some detail; from its origin and the timing of crystallisation (Honegger et al., 1982; Weinberg et al., 2000; Rolland et al., 2002; Singh et al., 2007; St. Onge et al., 2010) to its emplacement (Jowhar, 2001; Singh et al., 2007) and exhumation history (Choubey, 1987; Kirstein et al., 2006; 2009; Kumar et al., 2007) making it an ideal location to investigate the thermal evolution of part of the potentially dissected plateau region and question the apparent regional steady and slow denudation since the Eocene. Previous models of emplacement and exhumation are complex and vary significantly. They include northwards tilting of the batholith (Singh et al., 2007), slow steady exhumation (Kumar et al., 2007), rapid Early Miocene exhumation and south directed thrusting of the batholith along a northward dipping structure (Kirstein et al., 2006) and, southward tilting of the batholith in the Oligocene - Miocene (Kirstein et al., 2009).

Amphiboles are increasingly used as geobarometers particularly for calc-alkaline rocks (e.g. Schmidt, 1992) to yield pressure and hence depth of emplacement estimates for plutonic rocks. The Al-in-hornblende barometer is specifically calibrated for the assemblage quartz + alkali feldspar + plagioclase + hornblende + biotite + iron oxide + titanite + melt + fluid (Schmidt, 1992; Anderson and Smith, 1995) and is ideal for application to the granites and granodiorites of Ladakh. Here we present new amphibole compositional data from five samples across the Ladakh Batholith and recalculate previously published depth of emplacement data (Jowhar, 2001; Singh et al., 2007) using the Al-in-hornblende equation of Anderson and Smith (1995) which incorporates the effect of temperature for samples of appropriate bulk mineral assemblage (Table 1, 2).

As a result it is timely to present an inclusive model, which incorporates new emplacement depth calculations with available crystallisation and thermochronometry data so that the exhumation of the batholith from depth to the surface can be documented and integrated within the available tectonic framework.

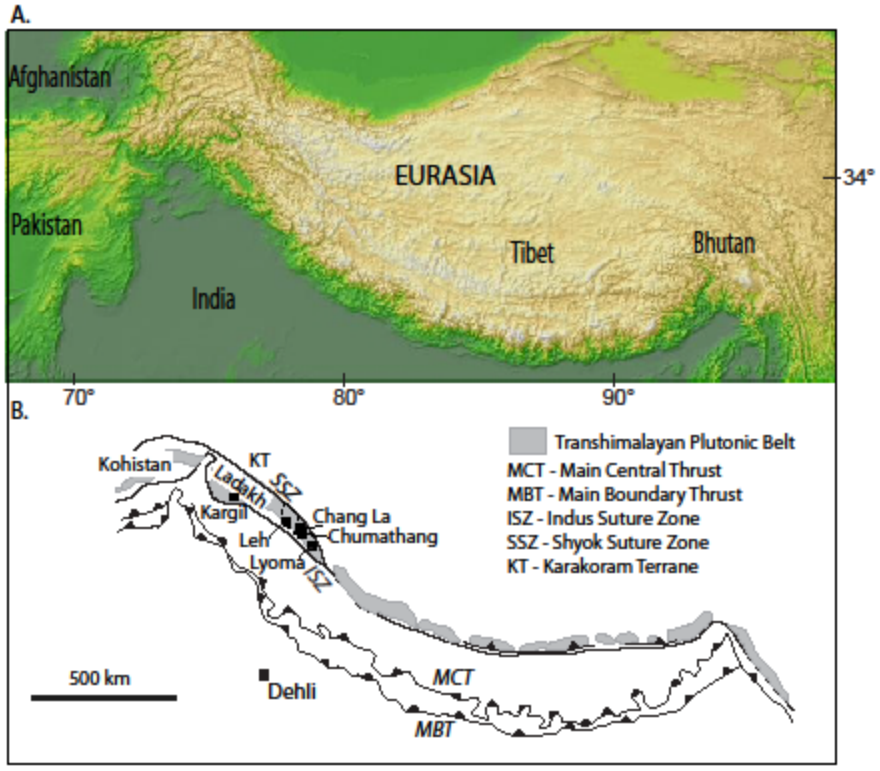

Figure 1. A. Digital elevation model of Himalayan region stretching from Afghanistan in the west to Bhutan in the east highlighting the spectacular change in relief from low lying Indian Plate (dark green) across the Himalayan mountain chain (yellow/white) and north into Eurasia. B. Sketch of principle structures in the region including from south to north the Main Boundary Thrust (MBT), Main Central Thrust (MCT), the Indus Suture Zone (ISZ) and the Shyok Suture Zone (SSZ). Dashed square indicates field area.

2. Geological setting

The calc-alkaline Andean-type Ladakh Batholith intrudes the Kohistan-Ladakh island arc terrane, which was sandwiched between Eurasia (the Karakoram terrane) and India during collision in the Paleogene (~50 Ma) (Fig. 1). The Ladakh Batholith intrudes thick sedimentary units of Aptian-Albian age with minor limestones inter-layered in the upper parts with andesitic flows (Rolland et al., 2002). The andesites form part of the Khardung Volcanic Formation (68-63 Ma) that dip 30-60° north-northeast and are locally deformed (Weinberg et al., 2000). The batholith is bound to the south by the Indus Suture Zone (ISZ) which mainly

separates it from the deformed sedimentary successions of the Indus Molasse and the High Himalaya. The Indus River follows the suture zone in the region of interest. The southern margin of the batholith is commonly onlapped by Tertiary sedimentary rocks of the Indus Group thrust northwards since Miocene times (Garzanti and van Haver, 1988). Where the molasse sits unconformably on the batholith the dip of this molassic strata is 30° S e.g. at Chumathang (St.-Onge et al., 2010).

U-Pb crystallization ages range from 103 to 47 Ma and are similar across the Transhimalayan Batholith (Honegger et al., 1982; Weinberg and Dunlap, 2000; Singh et al., 2007; Ravikant et al., 2009; St-Onge et al., 2010). Mid Cretaceous (Albian) ages have been measured in the region around Kargil (Honegger et al., 1982) (Fig. 1). Recent U-Pb SHRIMP zircon age dating indicates major plutonism in the Ladakh region between 70 and 50 Ma (Weinberg and Dunlap, 2000; Singh et al., 2007; Ravikant et al., 2009). Sheeted dykes were intruded in the last phase of magmatic activity in the Eocene ~46 Ma (Sorkhabi et al., 1994; Weinberg and Dunlap, 2000; St-Onge et al., 2010). Interestingly the limited number of samples from the batholith dated by U-Pb indicate that the Leh pluton is the youngest main magmatic phase (~50 Ma) with older U-Pb ages further north (~58-70 Ma) (Weinberg and Dunlap, 2000; Ravikant et al., 2009). There may be an east-west gradient in crystallisation age with the oldest intrusions in the west (Honegger et al., 1982).

The batholith is considered undeformed on a large scale but there is a diffuse deformation zone in the region north of Leh and a penetrative ductile shear fabric is developed within the Thanglasgo shear zone (Weinberg and Dunlap, 2000; Jain et al., 2003) (Fig. 2). Mylonitized gneiss is evident along the Leh-Khardung La route along with discrete shear zones with sub-horizontal and listric thrusts showing SW vergence (Jain et al., 2003; this study) suggesting some limited internal deformation.

3. Sampling and Petrology

We systematically sampled a region across the Ladakh Batholith to determine whether there was a clear spatio-temporal variation in emplacement history and thermal evolution. Twenty samples were collected from south to north across the region between 34.033°N 77.721 °E and 34.578°N 77.281°E (Fig. 1). These included diorites, granodiorites and granites. All samples have a modal mineralogy of quartz + two feldspar ± amphibole ± biotite ± accessory phases (sphene, zircon, apatite) ± iron oxides (Fig. 3). Where the igneous Al-in-hornblende geobarometer was applied the igneous buffering assemblage of quartz + alkali feldspar + plagioclase + hornblende + biotite ± Fe-oxides was identified for granodiorites and granites.

Table 1. Microprobe analyses of selected amphiboles from samples Disk 3320, Khars4349, Nang 4005, Tikse 3325 and Leh 3295 from across the Ladakh Batholith.

	Disk1	Disk2	Disk 3	Disk 4	Disk 5	Khar 1	Khar 2	Khar 3	Khar 4	Khar 5	Khar 6
SiO_2	46.10	46.73	47.06	46.52	45.69	46.36	45.20	45.44	46.02	47.06	46.79
TiO_2	1.39	1.10	1.52	1.29	1.42	1.21	1.40	1.44	1.54	0.92	1.34
Al_2O_3	6.38	5.89	6.07	6.08	6.39	6.71	7.19	6.92	7.07	6.56	6.40
Cr_2O_3	0.01	0.00	0.00	0.00	0.00	0.01	0.02	0.00	0.00	0.01	0.03
Fe_2O_3	9.38	7.66	9.61	9.68	9.02	6.12	7.16	6.82	5.83	7.18	6.38
FeO	11.14	13.17	12.53	11.69	11.81	10.01	10.20	9.52	10.56	9.68	9.21
MnO	0.31	0.31	0.46	0.36	0.29	1.57	1.50	1.56	1.48	1.47	1.49
MgO	10.78	10.25	9.62	10.28	10.60	11.98	11.36	12.02	11.73	12.07	12.55
CaO	10.26	10.74	10.29	10.24	10.35	11.18	11.07	11.21	11.24	11.22	11.19
Na_2O	1.72	1.26	1.02	1.43	1.85	1.27	1.30	1.30	1.20	1.11	1.19
K_2O	0.18	0.21	0.21	0.18	0.20	0.72	0.80	0.80	0.85	0.70	0.69
F	0.28	0.18	0.10	0.19	0.25	0.19	0.14	0.22	0.20	0.23	0.19
Cl	0.14	0.12	0.14	0.15	0.15	0.07	0.17	0.17	0.22	0.05	0.12
H_2O*	1.85	1.89	1.94	1.89	1.85	1.91	1.89	1.86	1.87	1.91	1.91
Total	99.75	99.41	100.51	99.87	99.74	99.20	99.31	99.14	99.67	100.06	99.36
Structural formulae											
Si	6.859	6.997	6.967	6.924	6.827	6.900	6.764	6.788	6.840	6.934	6.925
Al iv	1.119	1.003	1.033	1.067	1.125	1.100	1.236	1.212	1.160	1.066	1.075
Al vi	0.000	0.037	0.027	0.000	0.000	0.077	0.032	0.007	0.077	0.074	0.042
Ti	0.156	0.124	0.169	0.144	0.160	0.135	0.158	0.162	0.173	0.102	0.149
Cr	0.001	0.000	0.000	0.000	0.000	0.001	0.002	0.000	0.000	0.002	0.004
Fe^{3+}	1.050	0.863	1.071	1.084	1.014	0.686	0.806	0.767	0.652	0.797	0.711
Fe^{2+}	1.386	1.649	1.551	1.455	1.476	1.246	1.277	1.190	1.312	1.193	1.140
Mn	0.039	0.039	0.058	0.045	0.037	0.197	0.190	0.198	0.187	0.183	0.187
Mg	2.390	2.288	2.124	2.281	2.361	2.658	2.535	2.676	2.599	2.651	2.768
Ca	1.635	1.723	1.632	1.633	1.657	1.782	1.775	1.794	1.789	1.771	1.775
Na	0.497	0.367	0.292	0.414	0.535	0.366	0.378	0.375	0.346	0.318	0.341
K	0.034	0.040	0.040	0.034	0.038	0.137	0.152	0.152	0.161	0.131	0.131
(Ca+Na) (B)	2.000	2.000	2.000	2.000	2.000	2.000	2.000	2.000	2.000	2.000	2.000
Na (B)	0.365	0.277	0.292	0.367	0.343	0.218	0.225	0.206	0.211	0.229	0.225
(Na+K) (A)	0.166	0.131	0.040	0.080	0.231	0.285	0.305	0.321	0.296	0.220	0.246
$Mg/(Mg+Fe^2)$	0.633	0.581	0.578	0.611	0.615	0.681	0.665	0.692	0.664	0.690	0.708
$Fe^3/(Fe^3+Al^{vi})$	1.000	0.958	0.976	1.000	1.000	0.899	0.962	0.991	0.894	0.915	0.945
Sum of S2	13.00	13.00	13.00	13.00	13.00	13.00	13.00	13.00	13.00	13.00	13.00

	Leh 1	Leh 2	Leh 3	Leh 4	Leh 5	Leh 6	Leh 7	Leh 8	Leh 9	Leh 10
SiO_2	43.67	43.89	44.22	43.44	43.81	44.48	44.04	44.29	44.43	43.84
TiO_2	1.49	1.50	1.29	1.39	1.36	1.45	1.36	1.42	1.45	1.64
Al_2O_3	9.07	9.07	8.53	9.01	9.04	8.58	9.07	8.65	8.48	9.02
Cr_2O_3	0.01	0.02	-0.02	-0.02	-0.03	0.03	0.03	-0.04	-0.02	0.04
Fe_2O_3	5.54	5.25	5.54	6.17	5.16	5.47	6.38	4.93	6.14	5.35
FeO	14.06	14.22	13.62	13.43	14.26	13.99	13.40	14.07	12.95	14.23
MnO	0.52	0.57	0.57	0.57	0.53	0.58	0.66	0.55	0.48	0.62
MgO	10.00	9.92	10.38	10.09	9.96	10.30	9.99	10.25	10.75	9.97
CaO	11.80	11.69	11.84	11.70	11.85	11.83	11.63	11.98	11.84	11.85
Na_2O	1.19	1.23	1.09	1.19	1.14	1.21	1.15	0.97	1.09	1.16
K_2O	1.11	1.16	1.09	1.14	1.09	1.03	1.11	1.02	1.00	1.13
F	0.05	0.07	0.04	0.09	0.00	0.03	0.07	0.03	0.06	0.08
Cl	0.00	0.00	0.00	0.00	0.00	0.00	0.00	0.00	0.00	0.00
H_2O*	1.98	1.97	1.98	1.95	2.00	2.00	1.98	1.98	1.99	1.97
Total	100.46	100.55	100.15	100.12	100.18	100.95	100.84	100.09	100.61	100.86
Structural formulae										
Si	6.544	6.570	6.627	6.530	6.579	6.619	6.562	6.638	6.611	6.547
Al iv	1.456	1.430	1.373	1.470	1.421	1.381	1.438	1.362	1.389	1.453
Al vi	0.146	0.170	0.134	0.126	0.179	0.124	0.156	0.167	0.097	0.134
Ti	0.168	0.169	0.145	0.157	0.154	0.162	0.152	0.160	0.162	0.184
Cr	0.001	0.003	-0.002	-0.002	-0.004	0.004	0.004	-0.005	-0.002	0.005
Fe^{3+}	0.624	0.591	0.624	0.697	0.583	0.612	0.716	0.556	0.688	0.601
Fe^{2+}	1.762	1.781	1.707	1.688	1.791	1.741	1.670	1.764	1.611	1.778
Mn	0.066	0.073	0.072	0.073	0.068	0.073	0.083	0.069	0.060	0.079
Mg	2.233	2.214	2.320	2.260	2.230	2.285	2.219	2.289	2.383	2.219
Ca	1.895	1.874	1.902	1.885	1.907	1.886	1.857	1.923	1.888	1.896
Na	0.346	0.358	0.316	0.347	0.333	0.350	0.334	0.282	0.315	0.337
K	0.213	0.221	0.207	0.218	0.209	0.195	0.210	0.195	0.191	0.214
(Ca+Na) (B)	2.000	2.000	2.000	2.000	2.000	2.000	2.000	2.000	2.000	2.000
Na (B)	0.105	0.126	0.098	0.115	0.093	0.114	0.143	0.077	0.112	0.104
(Na+K) (A)	0.454	0.454	0.425	0.449	0.449	0.431	0.401	0.400	0.394	0.447
$Mg/(Mg+Fe^2)$	0.559	0.554	0.576	0.572	0.555	0.568	0.571	0.565	0.597	0.555
$Fe^3/(Fe^3+Alvi)$	0.811	0.777	0.824	0.847	0.765	0.832	0.821	0.770	0.876	0.817
Sum of S2	13.00	13.00	13.00	13.00	13.00	13.00	13.00	13.00	13.00	13.00

	Nang 1	Nang 2	Nang 3	Nang 4	Nang 5	Nang 6	Nang 7	Nang 8	Nang 9	Nang10
SiO_2	46.92	46.26	46.00	46.33	46.10	46.39	46.26	46.01	46.33	45.70
TiO_2	1.19	1.23	1.32	1.35	1.48	1.33	1.33	1.16	1.33	1.38
Al_2O_3	6.63	7.35	7.40	6.99	7.13	7.32	7.17	7.38	7.24	7.41
Cr_2O_3	-0.01	0.02	-0.01	0.02	-0.02	0.03	-0.04	0.02	0.00	0.00
Fe_2O_3	7.62	7.23	7.57	7.70	7.32	5.94	7.41	6.98	6.18	7.47
FeO	9.08	9.73	9.23	8.82	9.73	10.79	9.81	9.99	10.63	10.03
MnO	1.64	1.54	1.59	1.77	1.63	1.62	1.59	1.61	1.61	1.54
MgO	12.37	11.91	12.01	12.28	11.93	11.72	11.84	11.82	11.63	11.63
CaO	11.59	11.38	11.19	11.31	11.39	11.59	11.32	11.54	11.43	11.30
Na_2O	0.91	1.20	1.34	1.25	1.20	1.16	1.22	1.15	1.17	1.30
K_2O	0.62	0.74	0.77	0.68	0.75	0.79	0.77	0.76	0.74	0.79
F	0.12	0.13	0.17	0.09	0.13	0.10	0.14	0.18	0.15	0.08
Cl	0.00	0.00	0.00	0.00	0.00	0.00	0.00	0.00	0.00	0.00
H_2O*	1.99	1.98	1.96	2.00	1.98	1.99	1.98	1.95	1.96	2.00
Total	100.61	100.65	100.46	100.56	100.70	100.72	100.73	100.45	100.34	100.60
Structural formulae										
Si	6.871	6.795	6.767	6.800	6.779	6.823	6.798	6.784	6.836	6.742
Al iv	1.129	1.205	1.233	1.200	1.221	1.177	1.202	1.216	1.164	1.258
Al vi	0.016	0.068	0.051	0.009	0.014	0.093	0.040	0.066	0.095	0.030
Ti	0.131	0.136	0.146	0.149	0.164	0.147	0.146	0.128	0.147	0.153
Cr	-0.001	0.003	-0.002	0.002	-0.002	0.003	-0.005	0.002	0.000	0.000
Fe^{3+}	0.839	0.799	0.838	0.850	0.810	0.657	0.820	0.775	0.686	0.829
Fe^{2+}	1.112	1.196	1.136	1.083	1.197	1.328	1.206	1.231	1.312	1.237
Mn	0.204	0.191	0.198	0.219	0.202	0.202	0.198	0.201	0.201	0.192
Mg	2.700	2.607	2.633	2.687	2.614	2.570	2.595	2.597	2.558	2.558
Ca	1.818	1.792	1.764	1.779	1.794	1.826	1.782	1.823	1.807	1.785
Na	0.260	0.341	0.383	0.355	0.342	0.330	0.346	0.329	0.334	0.373
K	0.117	0.138	0.144	0.128	0.140	0.148	0.144	0.143	0.139	0.149
(Ca+Na) (B)	2.000	2.000	2.000	2.000	2.000	2.000	2.000	2.000	2.000	2.000
Na (B)	0.182	0.208	0.236	0.221	0.206	0.174	0.218	0.177	0.193	0.215
(Na+K) (A)	0.195	0.271	0.290	0.262	0.277	0.304	0.272	0.295	0.281	0.307
$Mg/(Mg+Fe^2)$	0.708	0.686	0.699	0.713	0.686	0.659	0.683	0.678	0.661	0.674
$Fe^3/(Fe^3+Alvi)$	0.982	0.921	0.943	0.990	0.983	0.877	0.954	0.921	0.879	0.966
Sum of S2	13.00	13.00	13.00	13.00	13.00	13.00	13.00	13.00	13.00	13.00

	Tikse 1	Tikse 2	Tikse 3	Tikse 4	Tikse 5	Tikse 6	Tikse 7	Tikse 8	Tikse 9	Tikse10
SiO_2	44.58	45.94	46.14	44.36	44.22	45.92	45.22	44.94	42.01	45.40
TiO_2	1.42	1.21	1.01	1.60	1.50	1.20	1.35	1.50	1.89	1.14
Al_2O_3	9.50	8.79	8.34	9.75	10.03	8.48	8.95	9.46	11.45	8.86
Cr_2O_3	0.02	0.03	0.05	0.00	0.00	-0.04	0.06	0.06	0.01	-0.01
Fe_2O_3	7.97	7.00	6.05	6.79	6.58	6.72	9.40	7.21	5.75	7.67
FeO	9.26	9.67	11.12	10.87	10.57	10.16	7.77	9.57	12.21	9.11
MnO	0.60	0.72	0.60	0.63	0.67	0.62	0.69	0.66	0.64	0.57
MgO	11.66	12.06	11.88	11.14	11.18	12.15	12.17	11.87	10.13	12.17
CaO	11.16	11.56	11.98	11.58	11.51	11.81	11.10	11.56	11.77	11.42
Na_2O	1.54	1.27	1.04	1.35	1.44	1.21	1.32	1.38	1.54	1.35
K_2O	0.58	0.48	0.59	0.64	0.60	0.46	0.50	0.50	0.86	0.51
F	0.09	0.04	0.03	0.01	0.01	0.06	0.10	0.07	0.11	0.03
Cl	0.00	0.00	0.00	0.00	0.00	0.00	0.00	0.00	0.00	0.00
H_2O*	2.00	2.04	2.03	2.03	2.03	2.02	2.01	2.02	1.96	2.03
Total	100.34	100.78	100.87	100.73	100.33	100.75	100.57	100.78	100.27	100.24
Structural formulae										
Si	6.548	6.697	6.751	6.525	6.519	6.708	6.596	6.568	6.271	6.653
Al iv	1.452	1.303	1.249	1.475	1.481	1.292	1.404	1.432	1.729	1.347
Al vi	0.193	0.208	0.190	0.215	0.261	0.169	0.135	0.197	0.284	0.184
Ti	0.156	0.132	0.111	0.177	0.166	0.132	0.148	0.165	0.212	0.126
Cr	0.002	0.003	0.006	0.000	0.000	-0.004	0.007	0.007	0.001	-0.001
Fe^{3+}	0.882	0.768	0.666	0.751	0.730	0.739	1.031	0.793	0.645	0.845
Fe^{2+}	1.138	1.179	1.361	1.337	1.303	1.241	0.948	1.170	1.524	1.117
Mn	0.074	0.089	0.074	0.078	0.083	0.077	0.086	0.082	0.081	0.071
Mg	2.554	2.621	2.591	2.442	2.457	2.646	2.646	2.586	2.253	2.659
Ca	1.757	1.806	1.878	1.825	1.818	1.848	1.735	1.810	1.883	1.794
Na	0.439	0.359	0.296	0.385	0.410	0.342	0.374	0.392	0.446	0.384
K	0.108	0.089	0.110	0.120	0.113	0.085	0.092	0.093	0.164	0.095
(Ca+Na) (B)	2.000	2.000	2.000	2.000	2.000	2.000	2.000	2.000	2.000	2.000
Na (B)	0.243	0.194	0.122	0.175	0.182	0.152	0.265	0.190	0.117	0.206
(Na+K) (A)	0.304	0.254	0.285	0.331	0.341	0.276	0.201	0.295	0.492	0.274
$Mg/(Mg+Fe^2)$	0.692	0.690	0.656	0.646	0.653	0.681	0.736	0.689	0.597	0.704
$Fe^3/(Fe^3+Alvi)$	0.820	0.787	0.778	0.778	0.737	0.814	0.885	0.801	0.694	0.821
Sum of S2	13.00	13.00	13.00	13.00	13.00	13.00	13.00	13.00	13.00	13.00

Table 2 Average pressure and depth calculations for new and published amphibole mineral analyses.

Sample	Elevation (m)	Longitude (°)	Latitude (°)	Depth (km)	Pressure (kbar)	Distance north of Indus (km)
Leh3295	3295	77.526	34.119	14.1	3.88 ± 0.81	0.1
Tikse3328	3328	77.666	34.058	14.9	4.12 ± 0.94	1.4
LB15^{+}	4241	77.816	33.967	10.9	3.02 ± 1.05	8.8
JL29*	3750	77.583	34.188	12.4	3.29 ± 0.59	9.6
LB14^{+}	4409	77.819	33.967	9.15	2.42 ±0.96	10.0
Nang4300	4005	77.773	34.070	9.27	2.58 ± 0.78	10.6
JM85*	3800	77.853	33.988	8.64	2.29 ± 0.65	13.4
LB13^{+}	4742	77.867	33.998	9.02	2.39 ± 0.79	15.1
Khars4349	4349	77.616	34.226	8.81	2.33 ± 0.66	15.1
LB11^{+}	5060	77.914	34.017	6.49	1.72 ± 0.55	20.2
JM119*	5100	77.646	34.276	8.18	2.17 ± 0.41	20.9
JM91*	5290	77.937	34.036	6.66	1.76 ± 0.38	23.3
LB10^{+}	5301	77.944	34.075	8.77	2.32 ± 0.53	25.8
Disk3320	3320	77.569	34.544	7.00	1.85 ± 0.48	45.9

T = 710 °C for all samples. Depth calculation based on pressure = ρgh where g = 9.81 m/s^2, ρ = 2.7 x 10^3 kg/m^3 and h = depth in meters. Error on pressure analyses includes within sample compositional variation and potential variations in crystallisation temperature (670 – 730° C).
*Jowhar 2001; * Singh et al., 2007.

Igneous textures vary from medium- to coarse- grained and all samples are porphyritic to equigranular in nature (Fig. 3). Plagioclase and alkali feldspar are ubiquitous. Quartz (10-40%) varies from subhedral to anhedral and commonly shows strained extinction. Graphic intergrowth of quartz and alkali feldspar is evident in some samples. Plagioclase (30-40%) is euhedral to subhedral. Occasional zoning is observed as well as polysynthetic twinning in some phenocrysts. In addition the alkali feldspars (5-20%) show microcline cross hatched twinning and perthite intergrowth textures. Sericitisation of the feldspars is common particularly in the cores. Amphibole which is mainly hornblende accounts for ~25-5% of the assemblage in samples where it is present. It is pleochroic, subhedral, occasionally twinned and commonly associated with titanite. Biotite (<10%) is the other common ferromagnesian mineral present and is euhedral and pleochroic (Fig. 3). Occasionally it is intergrown with relict amphibole. Some alteration to chlorite is evident. Apatite and zircon have magmatic habits and are generally elongate with two terminations.

4. Results

4.1 Mineral analyses

Amphiboles from 5 samples across the Ladakh Batholith (Leh, Tikse, Nang, Khars and Disk (Fig. 2)) were analysed using a CAMECA SX100 microprobe at the University of

Edinburgh. Mineral analyses are presented in Table 1. Cations were initially calculated on the basis of 23 oxygens and then recalculated to account for ferric iron. The measured amphibole compositional data are in excellent agreement with published data (Jowhar, 2001; Singh et al., 2007) (Fig. 3). In the B (=M4) site Ca varies from 1.632 to 1.924 and Na from 0.071 to 0.367. All are magnesio-hornblende/hornblende in composition (Fig. 3) with some iron enrichment and are similar in composition to those used in the empirical Al-in-hornblende geobarometer of Hammerstrom and Zen (1986). All suitable new and published compositional data have been used to estimate emplacement depths across the Ladakh Batholith (Table 2, Fig. 2).

4.2 Geobarometry and depth estimates

The geobarometer of Schmidt (1992) modified for the effect of temperature, which can greatly increase Al^{IV} in hornblende (Anderson and Smith, 1995), is applied here to samples from across the batholith. Using the equation of Anderson and Smith (1995) the pressure of crystallisation of the sampled Ladakh granites and granodiorites is estimated (Table 2). Crystallisation temperatures for the Ladakh Batholith were recalculated using the amphibole – plagioclase thermometer of Blundy and Holland (1990) and the data of Jowhar (2001). Crystallisation temperatures range from 730 °C to 670 °C with the lowest temperature only recorded by the granite sample (JM91) at Chang La. Pressures were calculated for temperatures varying between 730 and 670° C. Results of the average pressure and depth calculations at a temperature of 710°C are presented in Table 2. The error bars on the pressure estimate reflect both the temperature uncertainty and within sample compositional variability. The recalculated pressure and depth calculations from the studies of Jowhar, (2001) and Singh et al. (2007) vary from those previously published due to the temperature effect and the fact that Fe^{2+} and Fe^{3+} are calculated by charge balance and normalised amphibole composition to 13 cations. Samples with Na+Ca (M4) < 2.0±0.1 were not considered further due to potential alteration, this included LB17 (Singh et al., 2007). Note the position of sample LB18 could not be plotted as the co-ordinates provided (33°54.006', 77°46.891'; Singh et al., 2007) place the sample south of the Indus River. Finally only granodiorite/granite samples were included in the calculations since the geobarometers used are specifically calculated for these rock types (e.g. Hammerstrom and Zen, 1986).

Average pressure estimates vary from 4.1 kbar to 1.7 kbar (Table 2). Assuming the density of continental crust is 2.7×10^3 kg/m^3 emplacement depths of between ~15 and 6.5 km are estimated. Emplacement depth estimates decrease from ~15 – 11 km at distances <10 km north of the Indus River to ~6.5 - 9 km further north across the batholith (Fig. 2). This

suggests that the southern part of the batholith had more overlying rocks removed compared to the northern edge (Fig. 2).

The denudation history experienced across the batholith has been determined in a separate study for these and other samples using multiple low temperature thermochronometers (Kirstein et al., 2006; 2009). Here I summarise these data and other published thermochronometry results to demonstrate a spatially and temporally heterogeneous evolution for the Ladakh Batholith.

5. Discussion

5.1 Cooling history of the Ladakh Batholith

Low temperature thermochronology studies of the Ladakh Batholith aimed at understanding its thermal evolution are increasing (Choubey, 1987; Sorkhabi et al., 1994; Weinberg and Dunlap, 2000, Clift et al., 2002; Schlup et al., 2003; Kirstein et al., 2006; 2009; Kumar et al., 2007; van der Beek et al., 2009). Thermochronometric techniques that have been applied include $^{40}Ar/^{39}Ar$ (biotite, hornblende) dating; fission-track (titanite, zircon, apatite) dating and (U-Th)/He (zircon, apatite) dating. Each of these decay systems has a mineral specific closure temperature ranging from 350-600°C ($^{40}Ar/^{39}Ar$ - biotite, hornblende) to ~55-80°C (apatite He) (Fig. 4). Biotite and hornblende Ar-Ar cooling ages range from 52 to 44 Ma respectively (Weinberg and Dunlap, 2000; Clift et al., 2002) (Fig. 4). Fission-track dating of titanite yields an age range from 43-26 Ma, but mainly are in the range 30 ± 3 Ma (Choubey, 1987) (Fig. 4)

Zircon fission-track (ZFT) data are limited, with ages from the Kargil and Chang La areas (Fig. 1) indicating cooling from 46 – 41 Ma (Sorkhabi et al., 1994; Kumar et al., 2007), while ZFT ages from the Khardung and Lyoma regions are between 32 and 26 Ma (Kirstein et al., 2006; Kumar et al., 2007) (Fig. 4; 5). Zircon (U-Th)/He (ZHe) ages vary across the batholith, ranging from 31 Ma in the south to 14 Ma in the north (Kirstein et al., 2006; 2009) (Fig. 4). Apatite fission-track (AFT) ages are more extensive covering the region from Kargil to Chang La (Fig. 1). AFT ages range from 44 to 5 Ma (Choubey, 1987; Sorkhabi et al., 1994; Clift et al., 2002; Schlup et al., 2003; Kirstein et al., 2006; 2009; Kumar et al., 2007). The Pliocene ages are thought to be related to local shear related heating (Choubey, 1987). Yet, there remains an overall spread in single AFT ages from 44 to 6 Ma (Sorkhabi et al., 1994; Clift et al., 2002; Kirstein et al., 2006; 2009; Kumar et al., 2007) (Fig. 4). Finally apatite (U-Th)/He (AHe) ages range from 22 to 12 Ma (Kirstein et al., 2006; 2009). Combined these scattered

data may suggest rapid regional cooling in the Eocene (52 – 44 Ma) followed by slower cooling from the Late Eocene to present (Fig. 4). However thermal modelling of available fission-track length data from the Ladakh Batholith suggests otherwise (Kirstein et al., 2006; 2009).

Examining the exhumation history in detail results in a distinct geographic distribution of the low temperature thermochronometry ages being observed, with a systematic decrease in age with distance from the Indus River (Kirstein et al., 2009) (Table 3, Fig. 5). ZHe, AFT and AHe ages of samples along the southern margin of the batholith are consistently older than those from the central and northern region (Table 3, Fig. 5). All ages are younger than the Cretaceous-Tertiary U-Pb crystallization ages of the batholith (> 50 Ma - Weinberg and Dunlap, 2000; Singh et al., 2007; Ravikant et al., 2009). There is also considerable geographical variation in ages along strike of the ISZ (Kirstein et al., 2009; van der Beek et al., 2009). The northern batholith margin close to the Shyok Suture Zone has younger cooling ages with Middle Miocene ZHe (<18 Ma) and Late Miocene (<7 Ma) AFT ages (Kirstein et al., 2009).

Combining the available thermochronology datasets and assuming a geothermal gradient of 30°C/km and closure temperatures of 230°C, 180°C, 90°C and 55°C for the ZFT, ZHe, AFT and AHe thermochronometers respectively (Reiners et al., 2005) (Fig. 4) minimum exhumation rates can be calculated. For example, sample Khars5245 from the centre of the batholith has a ZFT age of 26.2 Ma and an AHe age of 12 Ma suggesting cooling from ~230°C to 55°C in ~14 Myr, yielding an exhumation rate of 0.4 km/Myr (Fig. 4). However, ZHe and AFT ages are within error for this and other samples from the central and southern parts of the batholith suggesting rapid cooling from ~ 180°C to 90°C (Fig. 4). This rapid cooling occurred earlier (~29 Ma) along the southern margin (e.g. sample Leh, Fig. 4) than in the central region (~22 Ma) (Khardung, Fig. 4). The thermochronometer dataset support a non- linear exhumation path in these regions with periods of rapid exhumation interspersed with periods of slower exhumation. Exhumation of the northern part of the Ladakh Batholith (samples Hund and Dok) occurred at a rate of ~0.4 – 0.6 km/Myr since Middle Miocene times (17-15 Ma) with more than 4 km of this material removed since ~7 Ma. However, along the southern margin < 2km of material has been removed since the Early Miocene (~19 Ma) (Fig. 4). The original models of the exhumation of the Ladakh Batholith need to be revised in light of these new combined data sets spanning crustal depths of 15 to ~2 km. In particular simple northward tilting alone as proposed by the pressure data (this study; Jowhar, 2001; Singh et al., 2007) is not sufficient to also explain the spread of the low temperature

Figure 2. A. Simplified geological map of the Ladakh field area with locations for key samples for which depth estimates have been calculated. JM and JL samples (filled squares) from Jowhar (2001); LB samples (open squares) – Singh et al. (2007); Open circles – this study. TSZ – Thansglasgo Shear Zone after Weinberg and Dunlap (2000). Chang La section stretches from LB15 to LB10. B. Calculated emplacement depths (from pressure data) plotted against distance north of the Indus River illustrating a clear geographic distribution with samples closer to the Indus River exhumed from greatest depth. Symbols as in 2A.

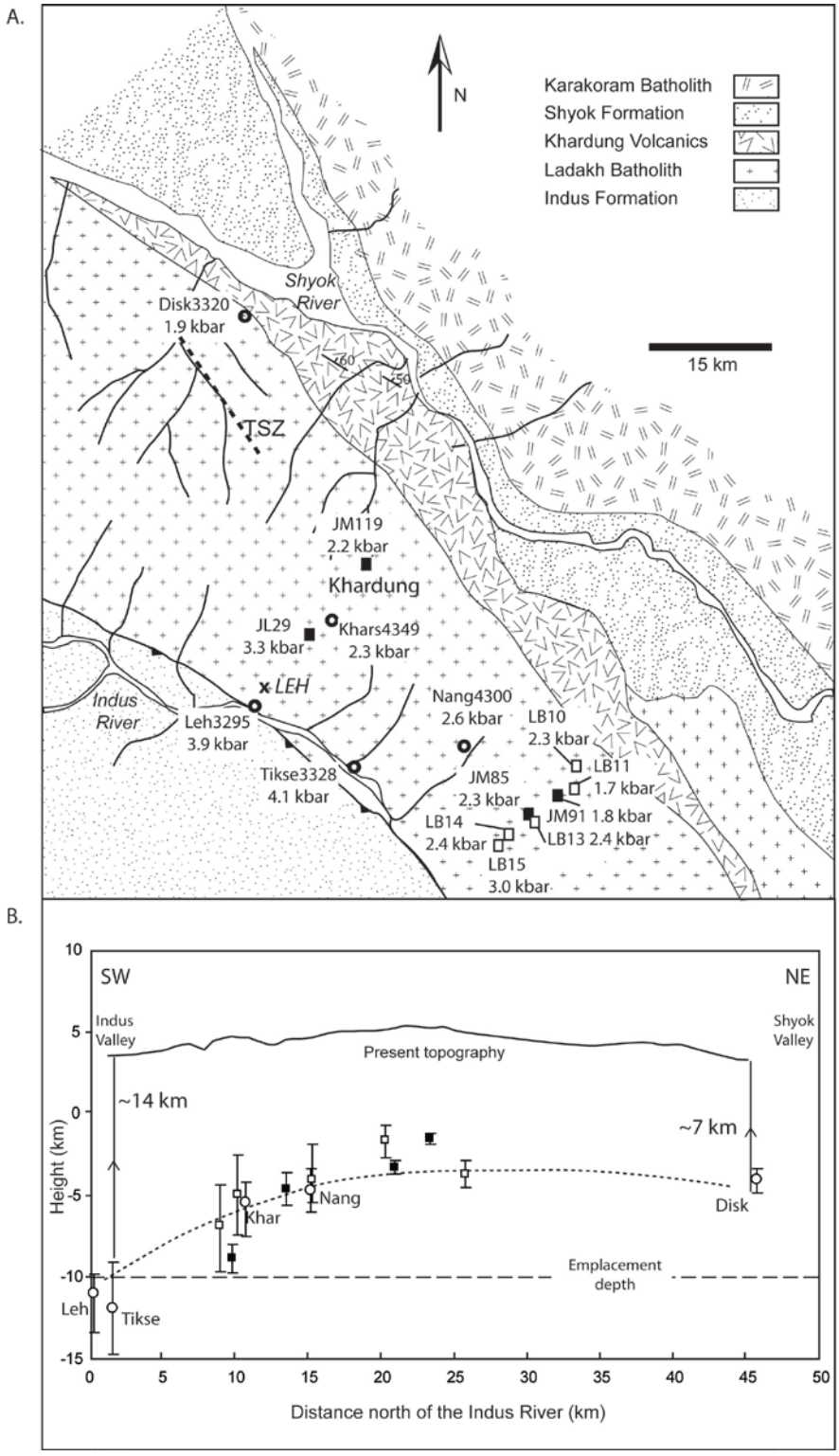

Figure 3. Photomicrograph illustrating mineralogy and texture of sample Leh3295. Plot of Al^{iv} versus Mg/(Mg+Fe) used to classify amphiboles indicating the magnesio-hornblende nature of the majority of new and recalculated amphibole analyses from the Ladakh Batholith (after Hammerstrom and Zen, 1986).

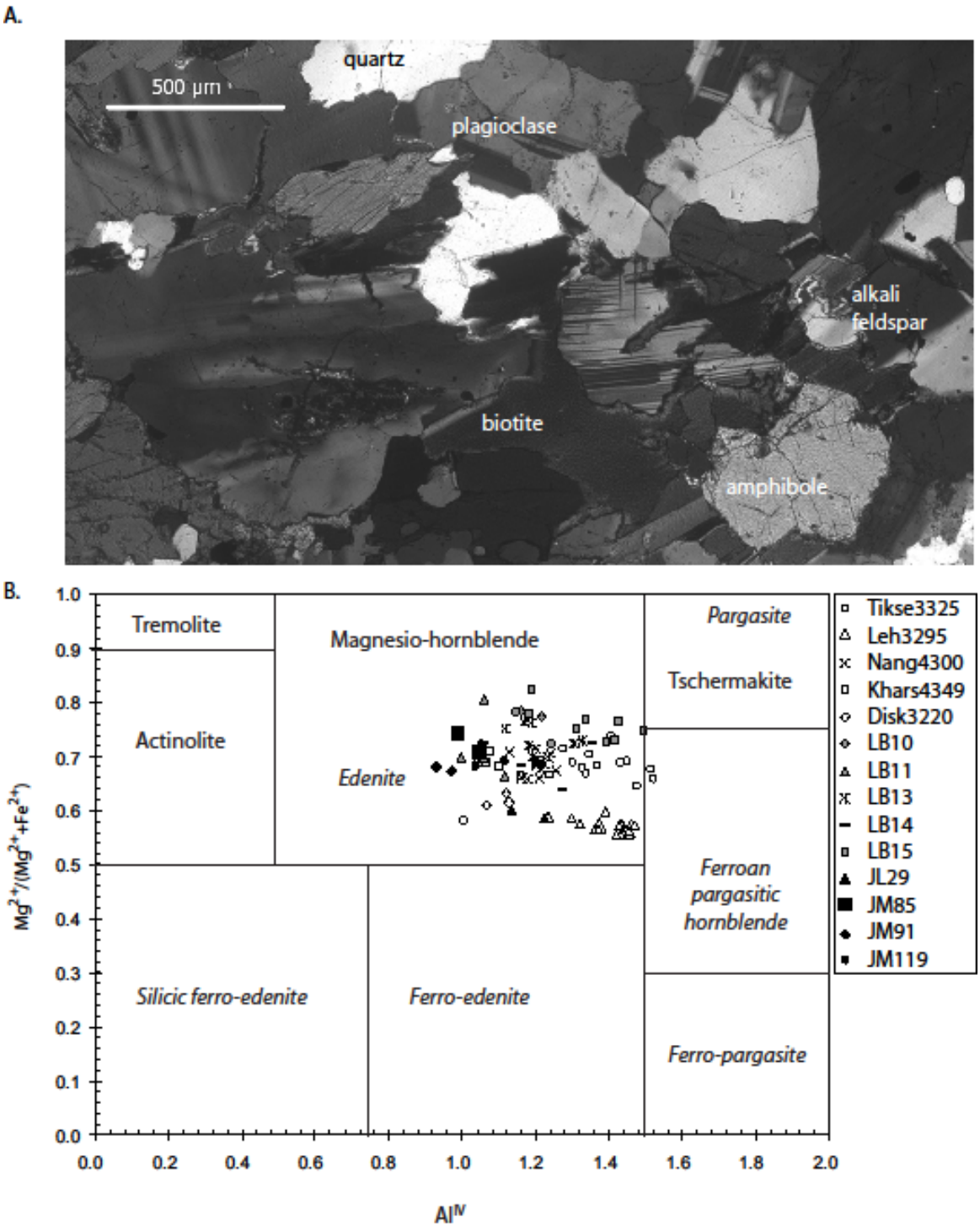

Figure 4. Plot of closure temperature versus age for all thermochronometers applied to different parts of the Ladakh Batholith. Crystallisation ages (thick black line) range from 50 to 70 Ma predominantly (St. Onge et al., 2010) and combined with the Ar-Ar ages (52 – 44 Ma) suggest rapid cooling in the Eocene. Note considerable array of ages for other thermochronometers including AFT dating. Closure temperatures based on summary in Reiners et al. (2005). Selected individual data plotted for Chumathang (Choubey, 1987; St. Onge et al., 2010), Leh (Clift et al., 2002; Kirstein et al., 2009; Schärer et al., 1984; Weinberg and Dunlap, 2000), Khardung (Kirstein et al., 2006) and Kargil (Sorkhabi et al., 1994; U-Pb age 101 ± 2 Ma (Schärer et al., 1984) not plotted) to demonstrate geographic variability in cooling history. Error bars plotted for each analysis except where error is less than symbol size. Exhumation rates calculated assuming geothermal gradient of 30°C/km.

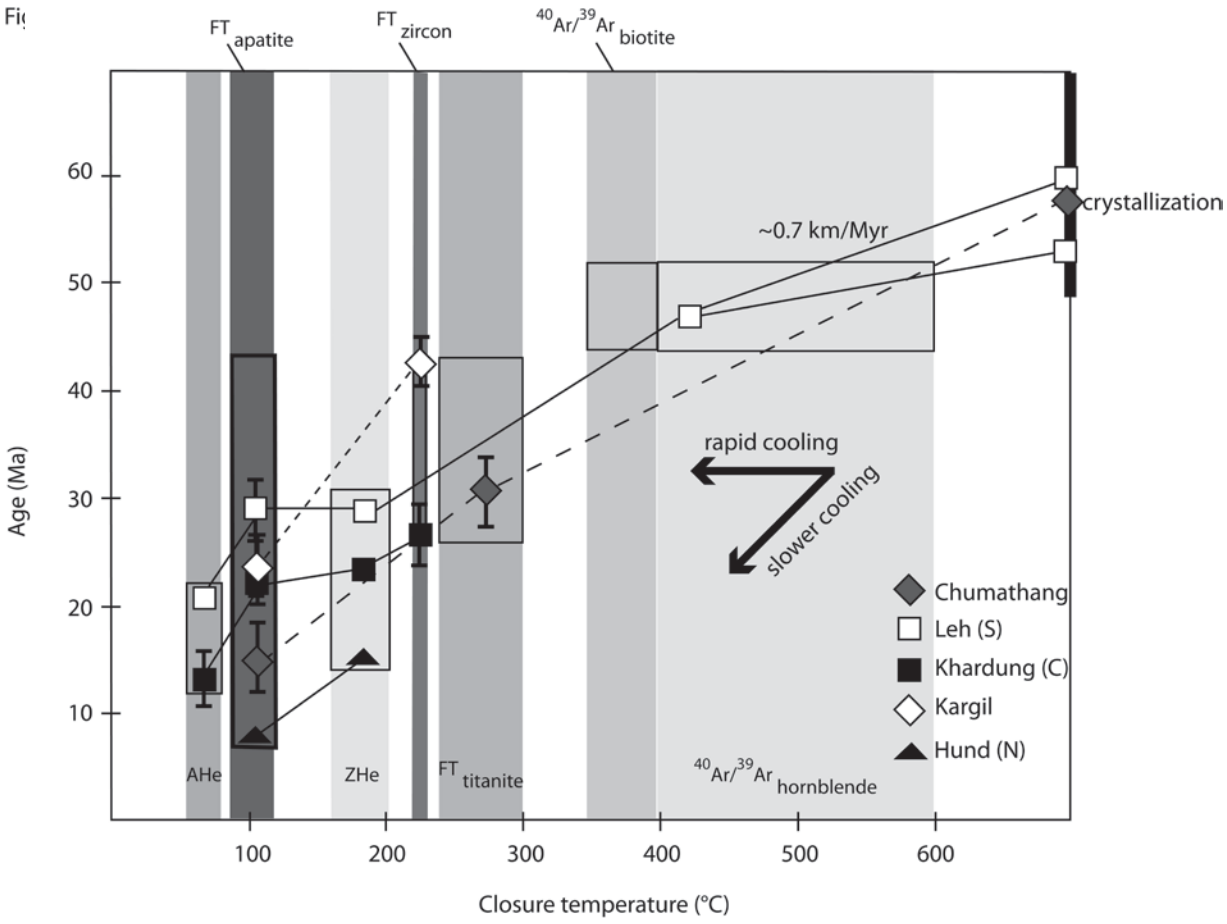

Figure 5. A. Distribution of samples discussed in this study (open circles). Zircon fission track data (grey boxes) indicating large variation in cooling ages from Eocene to Miocene (Kirstein et al. 2006; Kumar et al. (2007). Filled sample Khars5245 dated at 26.2 Ma (Kirstein et al., 2006); Open squares dated at 41.7 Ma and 43.7 Ma (Kumar et al., 2007). B. ZHe, AFT and AHe data from Kirstein et al. (2009). Note the significant geographic distribution of ages, with ages for all low temperature thermochronometers decreasing with distance north of the Indus River (modified from Kirstein et al., 2009).

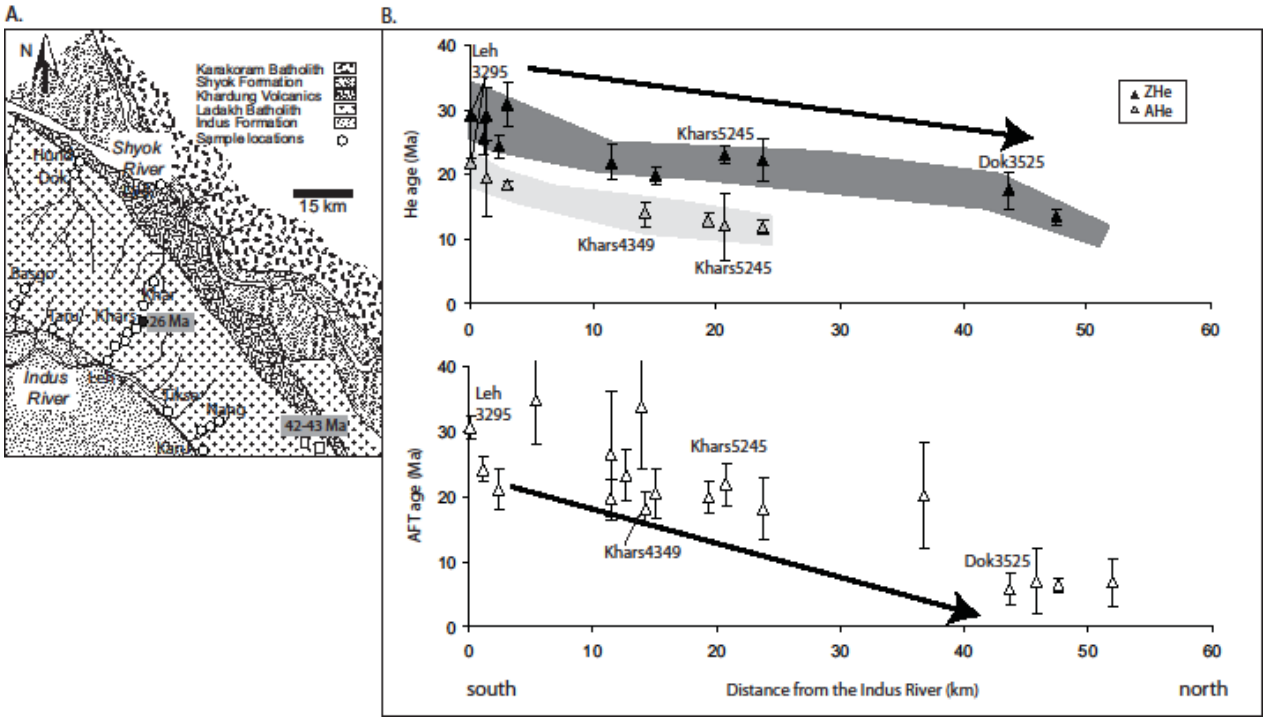

thermochronometry data. Northward tilting would potentially increase relief along the southern batholith margin resulting in the greatest exhumation (~14 km) in this region, yet the AFT cooling ages suggest that the southern part of the batholith was exhumed to within ~3-4 km of its current level by Oligocene times (~29 Myr). Southwards tilting alone post-dating emplacement would predict exhumation from greatest depth along the northern margin which is clearly not the case. The new data support a model in which northwards tilting shortly after emplacement lead to erosion and exhumation of the southern part of the batholith. Palaeogene foreland basin deposits in northwest India indicate a volcano-sedimentary source consistent with uplift and erosion of the Ladakh-Kohistan arc (Najman and Garzanti, 2000). This was followed by southwards tilting and subdued erosion of the southern margin. In the following section the potential impact of continent-continent collision and consequent thrust tectonics and crustal melting on the topography will be discussed to generate an integrated tectonic model of the phases of exhumation of the Ladakh Batholith since crystallisation.

5.2 Response to continent-continent collision

The timing of continental collision between India and Eurasia is well constrained in the NW Himalayas to be between 52 and 50 Ma which is co-incident with slowing down and erratic migration of the Indian Plate and the end of arc magmatism (Rowley, 1996; Treloar,

1997; Weinberg and Dunlap, 2000). Once subduction of the Neotethys oceanic crust was complete and continent-continent collision commenced, calc-alkaline magmatism ceased forming the Ladakh Batholith. The youngest U-Pb crystallisation ages document this last intrusive episode near Leh to be 49.8 ± 0.8 Ma (Weinberg and Dunlap, 2000). The Indian Plate has continued to move in a north-northeast direction at a rate of ~ 49 mm/year which has generated substantial crustal thickening and shortening both north and south of the ISZ (Treloar and Coward, 1991). Crustal thickening has resulted in the formation and intrusion of the Mango Gusar, Masherbrum and Baltoro plutons in the Karakoram region since the Miocene (Parrish and Tirrul, 1989). These plutons and the associated dykes highlight that this region was thermally anomalous with partial melt forming since ~ 25 Ma (Searle et al., 1998). To the south of the ISZ, strain accommodation associated with the collision, and continued northward migration, of India with Eurasia has been accommodated in the Himalaya in a number of ways including crustal thickening and the development of major structures. The Indus Group sediments south of the Ladakh Batholith are intensely deformed (Garzanti and van Haver, 1988; Clift et al., 2002). Early S- or SW- directed thrusts are related to crustal thickening and back thrusting as a result of the overall dominant compressional tectonic forcing (Searle et al., 1990). This early south-vergent phase of deformation was later overprinted by Miocene north-vergent deformation (Searle et al., 1990; Kirstein et al., 2006). The oldest south dipping faults in the Indus Molasse Chogdo Formation may be Oligo-Miocene in age (Cannat and Mascle, 1990; Mahéo et al., 2006). Finally southwards thrusting of the Karakoram terrane over the batholith is recorded by activity on the Main Karakoram Thrust, which is a Late Miocene breakback thrust (Rex et al., 1988).

5.3 Integrated tectonic model

The U-Pb crystallisation age of diorites and granodiorites from the southern and central part of the batholith vary, ranging between ~50 and 70 Ma (Weinberg and Dunlap, 2000; Singh et al., 2007; Ravikant et al., 2009) (Fig. 4). U-Pb crystallisation ages from Kargil are Cretaceous (~103 Ma; Honegger et al., 1982; Schärer et al., 1984), but given the sparse distribution of samples no clear systematic U-Pb age trend is observed. The new Al-in-hornblende geobarometry data indicate that the granites and granodiorites were emplaced at variable depths from 15 to 6.5 km during this time interval. Granodiorite sample LB10 was emplaced at a depth of ~9 km between ~58 and 60 million years ago (Singh et al., 2007), prior to final collision of India. Ar-Ar thermochronometry in hornblende and biotite indicates post-collisional cooling of the Ladakh Batholith to < 350 °C between 52 and 44 Ma (Weinberg and

Dunlap, 2000; Clift et al., 2002) (Fig. 4). This suggests rapid cooling of the batholith at a rate of ~21 °C/Myr (change in temperature = 900 - 350°C; duration = 70 – 44 Ma) in the early Cenozoic. Titanite fission-track and ZFT cooling ages vary from ~45 Ma to 26 Ma (Choubey, 1987; Sorkhabi et al., 1994; Kirstein et al., 2006; Kumar et al., 2007) and suggest that at least part of the batholith, at Kargil and Chang La, had cooled to <230° C in the Eocene (Fig. 4). An extensive recent study by Kirstein et al. (2009) in the region near Khardung reveals that ZHe, AFT and AHe ages vary systematically, decreasing in age with distance north of the Indus River (and hence ISZ) (Table 3).

Both the pressure of magma emplacement data and the low temperature thermochronometry data indicate asymmetry in the thermal history of the Ladakh Batholith. Initial topographic asymmetry may have resulted directly from collision of India with Eurasia. To the west, in Kohistan, an entire section through the arc-crust is revealed with deep granulites, amphibolites and plutonic rocks through to surface volcanic rocks and sediments exposed sequentially with distance north of the Main Mantle Thrust (Fig. 1). In Ladakh more than 8 km of material had been denuded from the southern margin and this part of the batholith was exhumed to within 2 km of the surface by ~18 Ma as revealed by AHe dating. In the central and northern parts less exhumation of the batholith had occurred at this time as ZHe and AFT ages vary from 25 to 6 Ma. By 12 Ma however, the central region had been exhumed to within 2 km of the surface while temperatures in the northern region were > 80°C until 6-7 Ma (Table 3). More than 2 km of material has been removed from this northern region since late Miocene times.

Combining the new geobarometry data presented here with the available thermochronometry data the Ladakh Batholith appears to have been tilted northwards initially and later southwards so that exhumation was asymmetric. To account for this ‘see-saw’ activity a new tectonic model is described in which the geometry of the plates following collision, the development of steps in the décollement on the main thrust fault together with crustal melting and differences in lithospheric properties between the Indian and Eurasian Plates played a significant role in the unroofing history of the batholith (Fig. 6). In this model, the batholith forms on the southern margin of Eurasia as a function of continued subduction of the Neotethys Ocean during the Early Cenozoic (Fig. 6a). Sediments to the north of the batholith preserve evidence of shallow marine conditions in the Cretaceous suggesting accretion of the batholith to the southern Eurasian margin post Albian times (Ehiro et al., 2007). The batholith was tilted on collision of India with Eurasia resulting in the steep dip

Table 3. Summary of published multiple low temperature thermochronometry data for region of Ladakh Batholith.

Sample	Longitude (°)	Latitude (°)	Distance to Indus (km)	ZFT (Ma) ± 2σ	ZHe (Ma) ± 2σ	AFT (Ma) ± 2σ	AHe (Ma) ± 2σ
Central region							
*Khars5245	77.605	34.279	20.7	26.2±3.6	23.0±1.4	21.9±3.2	12.0±5.1
*Khars5132	77.622	34.269	19.4			19.9±2.4	12.9±1.2
*Khars4552	77.617	34.241	15.1		19.9±1.4	20.5±3.8	
Khars4349	77.616	34.226	14.3			18.1±2.6	14.0±1.9
*Khars4110	77.619	34.212	12.7			23.3±4.0	
*Khars3921	77.611	34.202	11.5		21.9±2.7	26.4±9.8	
Nang3555	77.721	34.033	2.4		24.4±1.7	21.1±3.2	
Nang4300	77.794	34.086	11.5			19.8±2.8	
Khar4918	77.619	34.313	23.7		22.2±3.3	18.1±4.8	11.9±1.2
Khar3975	77.658	34.419	36.8			20.1±8.2	
Southern margin							
Bas 1	77.282	34.246	5.4			34.9±6.8	
Bas 4001	77.322	34.304	13.9			33.8±9.6	
Taru3593	77.398	34.185	3.0		30.9±5.8		18.5±0.6
Leh3295	77.527	34.119	0.1		29.2±0.1	30.6±3.4	21.8±0.5
Tikse3325	77.666	34.058	1.4		29.3±4.1		19.4±5.9
Karu3400	77.731	33.932	1.2		25.6±2.4	29.9±5.8	
Northern margin							
Hund3250	77.458	34.578	47.6		13.5±1.2	6.3±2.4	
Dok3525	77.445	34.553	43.7		17.5±2.9	5.7±4.8	
Disk3220	77.569	34.544	45.9			6.9±5.0	
Tiri3240	77.683	34.544	52.0			6.8±3.6	

Note: ZFT – zircon fission track; ZHe – zircon He; AFT – apatite fission track; AHe – apatite He. AFT ages are central ages. Data from Kirstein et al., 2006 indicated by *. All other data from Kirstein et al., 2009. Dark grey shading indicates samples for which pressure data is presented.

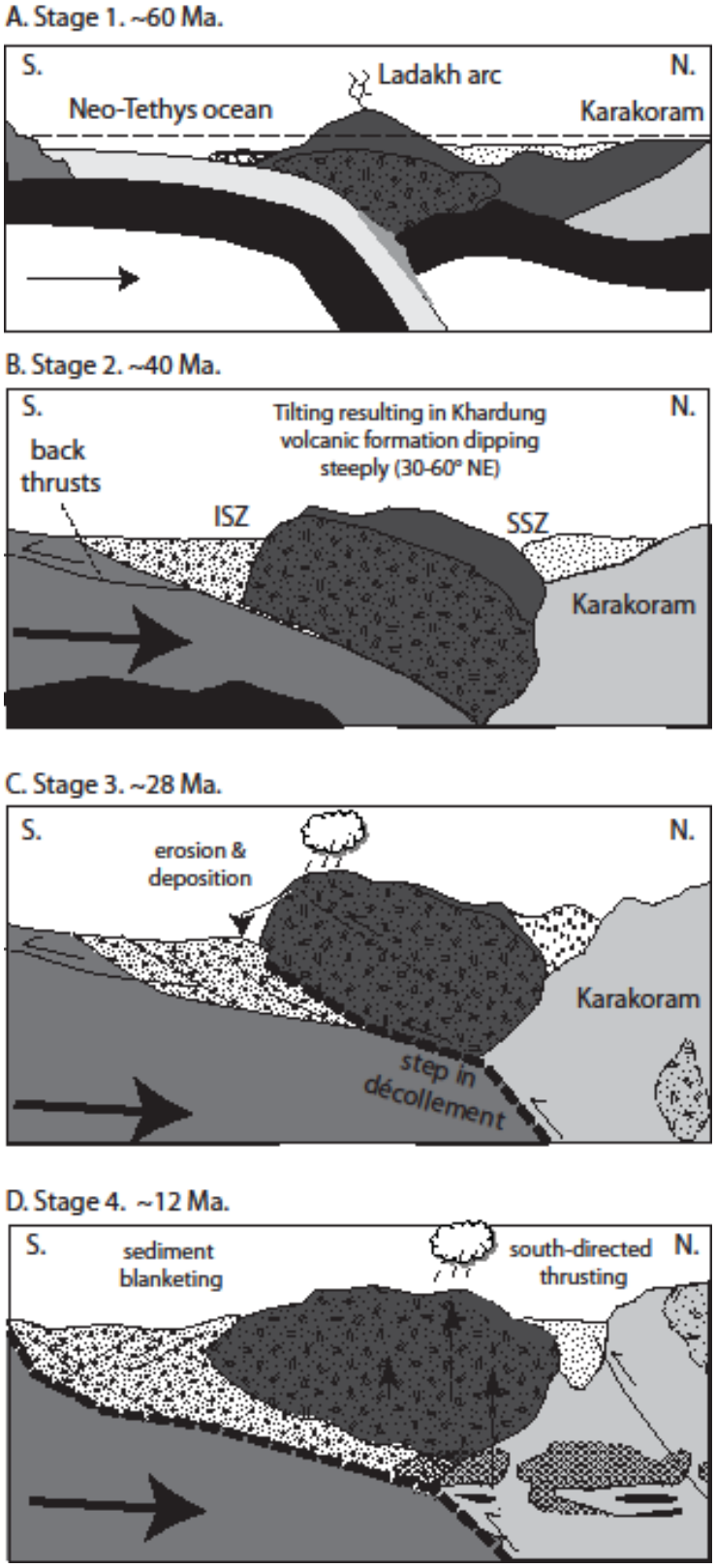

Figure 6. A. Subduction of the Neotethys oceanic crust and formation of the Ladakh island arc during the early Tertiary. B. Eocene collision and northwards tilting of the batholith. Rapid cooling to <350°C. Overlying extrusive Khardung Volcanic Formation dip steeply to the NNE (30-60°). C. Development of a thrust ramp geometry due to difference in lithospheric thickness and rock properties. Evidence of south-directed thrusting of the batholith is preserved in the Indus Group sediments. Progressive exhumation of the batholith from south to north. Melting initiated in the Karakoram terrane. D.Continued melting in the Karakoram terrane and exhumation of the northern margin. Mid Miocene thrusting, sedimentation and back-thrusting.

(30-60° NNE) of the Khardung Volcanic Formation (Fig. 6b). The batholith formed a competent structural block and acted as a buttress with little internal deformation. Cooling of part of the batholith occurred to < 250 ° C by ~42 Ma. To the south of the ISZ minor back-thrusts formed in shallow sediments on Indian crust. As collision progressed a step in the basal décollement potentially formed where there was a transition from relatively thin Indian continental crust and passive margin sediments to the thickened accreted island arc terrane (Fig. 6c). Such a step is evident in modern seismic and magnetotelluric studies of the Ladakh region (Arora et al. 2007; Rai et al., 2009). Using magnetotelluric data the ISZ has been imaged as a sub-vertical conductive structure, and to the north of the ISZ a north-dipping zone of low resistivity is imaged at the top of the underthrust Indian Plate consistent with fluids derived from underthrust sedimentary rocks (Arora et al., 2007). High crustal seismic attenuation in the Ladakh and Karakoram regions may result from aqueous fluids and/or partially molten crust (Rai et al., 2009).

These geophysical surveys support the theory that the difference in lithology, density and crustal thickness between the Indian Plate, accreted island arc and the Karakoram terrane were important in the structural evolution of the region (Fig. 6c). Space formed by tilting was filled by sediments and the batholith was pinned in the north by the thickened Karakoram terrane. A thrust-ramp geometry may have resulted and is consistent with the drainage morphology (short, steep profiles to the south; longer, less steep to the north). South-directed thrusts are evident in the Indus Group sediments (Chogdo and Sumda Formations) and are considered to be Oligo-Miocene in age (Mahéo et al., 2006). These thrusts potentially facilitated exhumation of the batholith. Evidence of batholith erosion is preserved within the Choksti and Hemis conglomerates of the Indus Group sediments (Garzanti and van Haver, 1988). The central part of the batholith was exhumed rapidly ~22 Ma when age invariant ZHe and AFT ages are recorded. This phase of rapid exhumation may be related to increased erosion coupled with southwards propagation of the crustal ramp.

Exhumation of the northern margin accelerated between 17 and 14 Ma. This unroofing may be related to further regional kinematic changes. From the middle Miocene leucogranite emplacement, uplift and exhumation of the Karakoram terrane is evident (Searle, 1996; Dunlap et al., 1998). The initiation of south directed thrusting of the Karakoram terrane over the northern batholith margin occurred in the Late Miocene. The northern margin was exhumed rapidly since 6-7 Ma with 3-4 km of material removed since that time, whereas further south <2 km has been removed since ~12 Ma suggesting asymmetric exhumation of the region.

6. Conclusions

Collision of the Indian and Eurasian plates in the Ladakh region resulted in initial northwards tilting of the Ladakh Batholith as evident from the variation in emplacement depths calculated using Al-in-hornblende barometry from south to north across the batholith. The variation in emplacement depths calculated across the Ladakh Batholith together with the observed dip of the overlying Khardung Volcanic Formation argues for northwards tilting of the batholith either during or post-dating collision. This northwards tilting resulted in elevated topography along the southern margin of the accreted island arc terrane which was preferentially eroded between 35 and 26 Ma. The development of S and SW directed thrusts in the Oligo-Miocene are consistent with changing regional stresses. The central part of the batholith was exhumed rapidly ~ 22 Ma (Kirstein et al., 2006). The resultant sediments potentially blanketed the lower surfaces of the southern margin and inhibited further erosion. The northern margin was exhumed at a rate of <0.4 mm/yr from ~18 Ma, reflected by the difference in the ZHe and AFT ages. During this time period north-directed thrusting of the Indus Molasse may have continued to mantle the southern margin with sediments limiting potential erosion as evident near Chumatang today. To the north the Karakoram terrane was thrust southwards along the Main Karakoram Thrust from ~10 Ma.

The plate geometry, the contrast in competency between the batholith and surrounding sediments and the major thrust detachment played a key role in the emplacement and exhumation history of the region. Given this proposed evolution topography must have been asymmetric throughout the Oligocene and Miocene and potentially only since the Pliocene has the current amplitude and wavelength of topography been established. Dismemberment of this southwestern extension of the Tibetan plateau in the Oligocene/Miocene may have influenced the observed variability along strike of the ISZ. Exhumation across the area was not slow and steady since the Eocene instead pulses of rapid denudation are recorded at ~30 Ma along the southern margin and at ~22 Ma towards the centre of the batholith linked to changes in relief.

Acknowledgements

This work was funded by a European Union Marie Curie fellowship HPMF-CT-2000-00515 to LAK. Field work and extensive discussions with Hugh Sinclair and Fin Stuart are gratefully acknowledged. David Steele and Chris Hayward are thanked for support during use of the microprobe. Roberto Weinberg, an anonymous reviewer and the editor, Fabrizio Storti, are thanked for their insightful reviews.

References

Anderson, J.L., Smith, D.R., 1995. The effects of temperature and fO_2 on the Al-in-hornblende barometer. American Mineralogist, 80: 549-559.

Arora, B.R., Unsworth, M.J., Rawat, G., 2007. Deep resistivity structure of the northwest Indian Himalaya and its tectonic implications. Geophysical Research Letters, 34: L04307, doi:10.1029/2006GL029165.

Blundy, J.D., Holland, T.J.B., 1990. Calcic amphibole equilibria and a new amphibole-plagioclase geothermometer. Contributions to Mineralogy and Petrology, 104: 208-224.

Cannat, M., Mascle, G., 1990 Réunion extraordinaire de la société géologique de France en Himalaya du Ladakh. Bulletin de la Société Géologique de France, 4: 553–582.

Choubey, V.M., 1987. Fission track geochronology of the southern part of the Ladakh batholith, Ladakh, northwest Himalaya. Geoscience Journal, VIII: 73-80.

Clift, P.D., Carter, A., Krol, M., Kirby, E., 2002. Constraints on India-Eurasia collision in the Arabian Sea region taken from the Indus Group, Ladakh Himalaya, India. In: P.D. Clift, Kroon, D., Gaedicke, C., Craig, J. (Editor), The tectonic and climatic evolution of the Arabian Sea region. Geological Society Special Publications, London, pp. 97-116.

de Sigoyer, J., Chavagnac, V., Blichert-Toft, J., Villa, I.M., Luais, B., Guillot, S., Cosca, M., Mascle, G., 2000. Dating the Indian continental subduction and collisional thickening in the northwest Himalaya: Multichronology of the Tso Morari eclogites. Geology, 28: 487-490.

Dunlap, W.J., Weinberg, R.F., and Searle, M.P., 1998, Karakoram fault zone rocks cool in two phases. Journal of the Geological Society: 155, 903-912.

Ehiro, M., Kojima, S., Sato, T., Ahmad, T., and Ohtani, T., 2007, Discovery of Jurassic ammonoids from the Shyok suture zone to the northeast of Chang La Pass, Ladakh, northwest India and its tectonic significance. Island Arc: 16, 124-132.

Garzanti, E. and Vanhaver, T., 1988. The Indus Clastics - fore-arc basin sedimentation in the Ladakh Himalaya (India). Sedimentary Geology, 59(3-4): 237-249.

Hammerstrom, J.M., Zen, E-A., 1986, Aluminum in hornblende: An empirical igneous geobarometer. American Mineralogist, 71, 1297-1313.

Honegger, K., Dietrich, V., Frank, W., Gansser, A., Thoni, M., Trommsdorff, V., 1982. Magmatism and metamorphism in the Ladakh Himalayas (the Indus-Tsangpo suture zone). Earth and Planetary Science Letters, 60: 253-292.

Jain, A.K., Singh, S., Manickavasagam, R.M., Joshi, M., Verma, P.K., 2003. HIMPROBE Programme: Integrated studies on geology, petrology, geochronology and geophysics of the Trans-Himalaya and Karakoram. Memoir of the Geological Society of India, 53: 1-56.

Jamieson, S.S.R., Sinclair, H.D., Kirstein, L.A., Purves, R.S., 2004. Tectonic forcing of longitudinal valleys in the Himalaya: morphological analysis of the Ladakh batholith, N. India. Geomorphology, 58: 49-65.

Jowhar, T.N., 2001. Geobarometric constraints on the depth of emplacement of granite from the Ladakh batholith, Northwest Himalaya, India. Journal of Mineralogical and Petrological Sciences, 96: 256-264.

Kirstein, L.A., Foeken, J.P.T., van der Beek, P., Stuart, F.M. and Phillips, R.J., 2009. Cenozoic unroofing history of the Ladakh Batholith, western Himalaya constrained by thermochronology and numerical modeling. Journal of the Geological Society London, 166: 667-678, doi: 10.1144/0016-7649.2008-107.

Kirstein, L.A., Sinclair, H., Stuart, F.M. and Dobson, K., 2006. Rapid Early Miocene exhumation of the Ladakh Batholith, northwestern Himalaya. Geology, 34: 1049-1052.

Kumar, R., Lal, N.,Singh, S. Jain, A.K., 2007. Cooling and exhumation of the Trans-Himalayan Ladakh batholith as constrained by fission track apatite and zircon ages. Current Science, 92: 490-496.

Mahéo, G., Fayoux X., H., Guillot, S., Garzanti, E., Capiez, P., Mascle, G., 2006. Relicts of an intra-oceanic arc in the Sapi-Shergol melange zone (Ladakh , NW Himalaya, India) : Implications for the closure of the Neo-Tethys Ocean. Journal of Asian Earth Sciences, 26: 695-707.

Najman, Y., Garzanti, E., 2000. Reconstructing early Himalayan tectonic evolution and paleogeography from Tertiary foreland basin sedimentary rocks, northern India. Geological Society of America Bulletin 112, 435– 449.

Parrish, R.P., Tirrul, R., 1989. U-Pb ages of the Baltoro granite, northwest Himalaya, and implications for monazite U-Pb systematics. Geology 17: 1076-1079.

Rai, S.S., Ashish, Padhi, A., Sarma, P.R., 2009, High crustal seismic attenuation in Ladakh-Karakoram. Bulletin of the Seismological Society of America, 99:407-415, doi:10.1785/0120070261.

Ravikant, V., Wu, F-Y., Ji, W-Q., 2009. Zircon U-Pb and Hf isotopic constraints on petrogenesis of the Cretaceous-Tertiary granites in eastern Karakoram and Ladakh, India. Lithos, 110, 153-166.

Reiners, P.W., Ehlers, T.A. Zeitler., P.K., 2005. Past, present and future of thermochronology. In Reiners, P.W., Ehlers, T.A. (editors) Low Temperature Thermochronology, 58, Reviews in Mineralogy and Geochemistry, 151-176.

Rex, A.J. et al., 1988. The geochemical and tectonic evolution of the Central Karakoram, North Pakistan [and Discussion]. Philosophical Transactions of the Royal Society of London. Series A, Mathematical and Physical Sciences, 326(1589): 229-255.
Rolland, Y. et al., 2002. The cretaceous Ladakh arc of NW Himalaya--slab melting and melt-mantle interaction during fast northward drift of Indian Plate. Chemical Geology, 182(2-4): 139-178.
Rowley, D.B., 1996. Age of initiation of collision between India and Asia: A review of stratigraphic data. Earth and Planetary Science Letters, 145(1-4): 1-13.
Schärer , U., Xu, R.H. and Allegre, C.J., 1984. U-Pb geochronology of Gangdese (Transhimalaya) Plutonism in the Lhasa-Xigaze Region, Tibet. Earth and Planetary Science Letters, 69(2): 311-320.
Schlup, M., Carter, A., Cosca, M., Steck, A., 2003. Exhumation history of eastern Ladakh revealed by ^{40}Ar-^{39}Ar and fission track ages: the Indus River-Tso Morari transect, NW Himalaya. Journal of the Geological Society, London, 160: 385-399.
Schmidt, M.W., 1992. Amphibole composition in tonalite as a function of pressure: An experimental calibration of the Al-in-hornblende barometer. Contributions to Mineralogy and Petrology, 110: 304-310.
Searle, M.P., 1996. Cooling history, erosion, exhumation and kinematics of the Himalaya-Karakoram-Tibet orogenic belt. In Harrison, T.M., Yin, A. (editors) The Tectonic Evolution of Asia, Cambridge University Press, 110-137.
Searle, M.P., Pickering, K.T. and Cooper, D.J.W., 1990. Restoration and evolution of the intermontane Indus Molasse Basin, Ladakh Himalaya, India. Tectonophysics, 174(3-4): 301-314.
Searle, M.P., Weinberg, R.F., Dunlap, W.J., 1998. Transpressional tectonics along the Karakoram fault zone, northern Ladakh: constraints on Tibetan extrusion. In Holdsworth, R.E., Strachan, R.A. and Dewey, J.F., (editors) Continental transpressional and transtensional tectonics, 135: London, Geological Society, Special Publication, 307-325.
Singh, S., Kumar, R., Barley, M.E. and Jain, A.K., 2007. SHRIMP U-Pb ages and depth of emplacement of Ladakh Batholith, Eastern Ladakh, India. Journal of Asian Earth Sciences, 30(3-4): 490-503.
Sorkhabi, R.B., Jain, A.K., Nishimura, S., Itaya, T., Lal, N., Manickavasagam, R.M., Tagami, T., 1994. New age constraints on the cooling and unroofing history of the Trans-Himalayan Ladakh Batholith (Kargil area), N.W. India. Proceedings of the Indian Academy of Science, 103: 83-97.

St-Onge, M.R., Rayner, N., Searle, M.P., 2010, Zircon age determinations for the Ladakh batholith at Chumathang (Northwest India): Implications for the age of the India–Asia collision in the Ladakh Himalaya. Tectonophysics, 495, 171-183.
Treloar, P.J., 1997. Thermal controls on early-Tertiary, short-lived, rapid regional metamorphism in the NW Himalaya, Pakistan. Tectonophysics, 273(1-2): 77-104.
Treloar, P.J., Coward, M.P., 1991. Indian Plate motion and shape: constraints on the geometry of the Himalayan orogen. Tectonophysics, 191, 189-198.
Van der Beek, P., Van Melle, J., Guillot, S., Pêcher, A., Reiners, P., Nicolescu, S., Latif, M., 2009. Eocene Tibetan plateau remnants preserved in the northwest Himalaya. Nature Geoscience, 2: doi:10.1038/NGE0503.
Weinberg, R.F., Dunlap, W.J., 2000. Growth and deformation of the Ladakh batholith, northwest Himalayas: Implications for timing of continental collision and origin of calc-alklaine batholiths. The Journal of Geology, 108: 303-320.
Weinberg, R.F., Dunlap, W. J., Whitehouse, M., 2000. New field, structural and geochronological data from the Shyok and Nubra valleys, northern Ladakh; linking Kohistan to Tibet. In: M.A. Khan, Treloar, P.J., Searle, M.P., Jan, M.Q. (Editor), Tectonics of the Nanga Parbat syntaxis and the western Himalaya. Geological Society of London, Special Publication, 170: 253-275.
Wen, D.-R. et al., 2008. Zircon SHRIMP U-Pb ages of the Gangdese Batholith and implications for Neotethyan subduction in southern Tibet. Chemical Geology, 252(3-4): 191-201.